Available online at www.sciencedirect.com
SCIENCE DIRECT®
Biosensors and Bioelectronics 19 (2004) 1377–1386
BIOSENSORS & BIOELECTRONICS
www.elsevier.com/locate/bios

Modeling and simulation of luminescence detection platforms

Khaled Salama*, Helmy Eltoukhy, Arjang Hassibi, Abbas El Gamal

Department of Electrical Engineering, Stanford University, Stanford, CA 94305, USA

Abstract

Motivated by the design of an integrated CMOS-based detection platform, a simulation model for CCD and CMOS imager-based luminescence detection systems is developed. The model comprises four parts. The first portion models the process of photon flux generation from luminescence probes using ATP-based and luciferase label-based assay kinetics. An optics simulator is then used to compute the incident photon flux on the imaging plane for a given photon flux and system geometry. Subsequently, the output image is computed using a detailed imaging sensor model that accounts for photodetector spectral response, dark current, conversion gain, and various noise sources. Finally, signal processing algorithms are applied to the image to enhance detection reliability and hence increase the overall system throughput. To validate the model, simulation results are compared to experimental results obtained from a CCD-based system that was built to emulate the integrated CMOS-based platform.

Keywords: Luminescence probes; Modeling; CMOS sensor; Post-processing

1. Introduction

Conventional biological assays are highly repetitive, labor intensive, and require microliter volume samples. The associated biochemical protocols often require days or weeks to perform at a cost of hundreds of dollars per test. Problems remain in detecting and quantifying low levels of biological compounds reliably, conveniently, safely and quickly. There is also a growing interest in the development of inexpensive portable biosensors for environmental and biomedical diagnostics. Solving these problems will require the development of new techniques and sensors, not only to selectively identify target compounds, but also to assay large numbers of samples.

A biochemical testing procedure can be divided into four steps: sample preparation, assay, detection, and data analysis as shown in Fig. 1. Currently, each step is being separately automated and miniaturized. However, there continues to be a need for designs that accommodate efficient integrated circuit manufacturing techniques to realize associated cost savings. We have been investigating the integration of three of these four steps into a single miniaturized platform as shown Fig. 2.

A variety of assay methods have been developed for molecular detection. These methods include electrochemistry (Woolley et al., 1998), optical absorption (Kunz, 1997), interferometry (Verpoorte et al., 1992), luminescence and fluorescence (Haugland, 1998). In this paper we focused on luminescence detection or luminometry. This technique is becoming increasingly popular due to its high sensitivity, wide dynamic range, and relatively inexpensive instrumentation. Superior sensitivity and low background distinguish luminometry from other analytical methods. Luminometry is up to five orders of magnitude more sensitive than absorption spectroscopy and more than 1000 times more sensitive than fluorometry. A state-of-the-art luminometer can detect as little as 0.6 pg of adenosine triphosphate (ATP) or 0.1 fg of luciferase (∼1100 molecules), two common luminescent analytes (Turner et al., 1985). Numerous bioluminescent and chemiluminescent reactions are studied using luminometry and are commonly used in biotechnology research, environmental testing, industrial applications, and clinical research. Among its many applications are the measurements of gene expression using reporter gene assays, the determination of intracellular ATP, and DNA sequencing.

Commercially available platforms for photon detection use bulky CCD camera-based setups and require the use of large quantities of reagents due to the light loss in the

* Corresponding author. Present address: Packard 257, 350 Serra Mall, Stanford, CA 94305, USA. Tel.: +1-650-725-9696; fax: +1-650-724-3648.
E-mail address: knsalama@stanford.edu (K. Salama).

0956-5663/$ – see front matter © 2004 Elsevier B.V. All rights reserved.
doi:10.1016/j.bios.2003.12.031

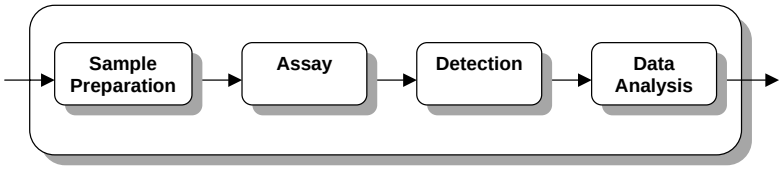

Fig. 1. General system currently used for biochemical testing.

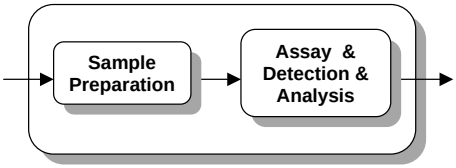

Fig. 2. Proposed system for future biochemical testing.

optical path. As a result these systems are not well suited to low cost applications. The development of imaging sensors in standard complementary metal-oxide-semiconductor (CMOS) technologies makes it possible to integrate sensing and processing on the same integrated circuit, enabling many low power and low cost applications. We have designed an integrated CMOS-based detection platform for use with luminescent microarrays. (Eltoukhy et al., 2004) A major concern in the design of such a miniaturized system is that the photogenerated signals can be very weak and therefore difficult to detect reliably. To quantify the detection limits of the envisioned system for the required assay concentration and throughput, we built a complete model for simulating the path from photogeneration through the optical path to detection and image post processing. Such modeling is used to guide the overall system design, whereby the special characteristics of a wide array of luminescent assaying methods can be exploited to enhance detection sensitivity beyond that of off-the-shelf CCD or CMOS-based sensors.

In Section 2, we describe the light generation process of luminescent probes and formulate the complete kinetic model of ATP-based and luciferase label-based assays. In Section 3, we describe the model of the proposed luminescent detection system including the associated optical pathway, imaging array characteristics, and applied signal processing algorithms. Finally, in Section 4, we present simulation and experimental results.

2. Luminescence light generation processes

Luminescence assay techniques are divided into two general categories. The first is direct target detection in which the photon emitting species physically interacts with the target of interest at a predetermined location. An example of this approach is luminescence-based immunoassays, which usually involve probing a protein of interest with a primary antibody that reacts with a secondary antibody. Light is produced when the enzyme bound to the secondary antibody acts upon a luminescent probe. The second category is indirect or linked detection in which the luminescent species indirectly measures the targeted characteristic, usually through an intermediate chemical process (Tang et al., 1995; Koster et al., 1997; Van Dyke et al., 2002; De Mello, 1996). While multiplexing is feasible in direct target detection, indirect detection requires confinement of the photon generation process as well as physical barriers for the independent reactions. This physical isolation complicates the integration of indirect detection methods to miniaturized systems, since high density mechanical barriers (e.g. micro-wells) as well as micro-scale solution delivery systems would be required. Since indirect detection is the more general of the two categories, it is the focus of the following analysis.

2.1. Luminescence light generation

The time-dependent light generation from a typical luminescence process is a function of the underlying chemical reaction kinetics. The rate of a reaction, in general, is the speed at which reactants are converted into products. If enzyme species E (the catalyst) converts the substrate molecule S into product P, the stoichiometric formula is given by

$$S + E \overset{k_f, k_r}{\leftrightarrow} E + P, \tag{1}$$

where k_f and k_r are the association and disassociation rate constants. In (1) the reaction rate is defined by

$$\text{rate} = \frac{\mathrm{d}[P]}{\mathrm{d}t} = -\frac{\mathrm{d}[S]}{\mathrm{d}t} = k_f[S][E] - k_r[E][P], \tag{2}$$

where $[E]$, $[S]$, and $[P]$ are the concentrations of the enzyme, substrate and product in the medium, respectively. Now if we suppose that the above process is a luminescence enzymatic reaction with quantum yield α, then the photon generation rate I in volume V of the reaction medium (A is Avogadro's number) would 'be

$$I = (\alpha VA)\frac{\mathrm{d}[P]}{\mathrm{d}t} = (\alpha VA)[E](k_f[S] - k_r[P]). \tag{3}$$

The total number of photons generated by this luminescence process N_{ph} (T), in the time interval T, would be

$$N_{ph}(T) = (\alpha VA)[E]\int_T (k_f[S] - k_r[P])\mathrm{d}t. \tag{4}$$

In luminescence assays the experiment is typically set up in such a way that the luminescence probe (e.g. a light generating enzyme) either reports the quantity of a substrate molecule (e.g. ATP) or the molecule to which it binds (e.g.

luciferase-based labels in immunoassays). The photon generation rate from the luminescence reaction, which is a function of the target concentration, is then measured and correlated to the target concentration.

2.1.1. Substrate detection kinetics

In the first group of luminescence assays, the rate at which photons are generated represents the substrate concentration given by (3). As the substrate is consumed by the catalyst, the light intensity decreases and eventually approaches zero. If we assume that the disassociation rate is insignificant (i.e. negligible inhibition), the light intensity with initial substrate concentration $[S_0]$ becomes

$$I(t) = (\alpha VA)\frac{\mathrm{d}[P(t)]}{\mathrm{d}t} = (\alpha VA)k_\mathrm{f}[E][S_0]\mathrm{e}^{-k_\mathrm{f}[E]t}. \quad (5)$$

The total amount of photons from time $t = 0$, the start of the process, to $t = T$ is

$$N_\mathrm{ph}(T) = (\alpha VA)[S_0](1 - \mathrm{e}^{-k_\mathrm{f}[E]T}). \quad (6)$$

The photon intensity in (6) is proportional to the target concentration, but the light intensity decays exponentially with a time constant, which is a function of the catalyst concentration and turnover rate k_f.

2.1.2. Catalyst detection kinetics

The second approach in luminescence assays is to link the target molecule quantity to a luminescence catalyst. In this approach, excess substrate is used, making sure that its consumption does not affect the reaction kinetics. If the saturation concentration for the substrate is $[S_\mathrm{max}]$ and the target concentration is equal to the catalyst $[E]$, the light intensity becomes

$$I(t) = (\alpha VA)\frac{\mathrm{d}[P(t)]}{\mathrm{d}t} = (\alpha VA)k_\mathrm{f}[S_\mathrm{max}][E]. \quad (7)$$

Since the light intensity based on (7) is time independent and proportional to the target (or the catalyst) concentration, the total number of photons generated from this process is a function of the integration time, i.e.

$$N_\mathrm{ph} = (\alpha VA)k_\mathrm{f}[S_\mathrm{max}][E]T. \quad (8)$$

In such assays, the number of target molecules can be very small resulting in a low but steady light. Long integration times, however, can be used to collect a significant number of photons.

2.2. Models of specific luminescent assays

2.2.1. ATP measurement

ATP bioluminescence assays are designed to measure the quantity of adenosine 5′-triphosphate (ATP) in a sample (Schena et al., 1995). Its applications include indirect measurement of bacteria, yeasts, fungi and other microorganisms, which have a regulated number of ATP in foodstuffs, beverages, water and other media. The assay typically employs recombinant luciferase to catalyze the reaction

$$\mathrm{ATP} + \text{luciferin} + \mathrm{O_2} \xrightarrow{\text{luciferase}} \mathrm{AMP} + \text{oxyluciferin} + \mathrm{CO_2} + \mathrm{PPi} + h\nu. \quad (9)$$

In most practical assays, the concentration of luciferin is high enough that we can consider it to be in deep saturation as shown in Fig. 3a. In this case, and when product inhibition is negligible, the rate of ATP consumption is given by

$$\frac{\mathrm{d}[\mathrm{ATP}]}{\mathrm{d}t} = -k_\mathrm{L}[E][\text{luciferin}_\mathrm{max}][\mathrm{ATP_0}]\mathrm{e}^{-k_\mathrm{f}[E][\text{luciferin}_\mathrm{mac}]t}, \quad (10)$$

where k_L is the association rate of luciferase macro-reaction. We can rewrite (10) by substituting $k_t = k_\mathrm{L}[E][\text{luciferin}_\mathrm{max}]$ as the turnover rate of the ATP consumption to obtain

$$I(t) = (\alpha VA)k_t[\mathrm{ATP_0}]\mathrm{e}^{-k_t t}. \quad (11)$$

The quantum efficiency of luciferase is about 0.88, and the turnover rate of the enzyme, depending on the ratio of luciferase to ATP, can vary from 0.1 to $1\,\mathrm{s}^{-1}$ (glow compared to flash). In the glow process, the light intensity is approximated by

$$I(t) \approx 5.3 \times 10^{22} V[\mathrm{ATP_0}]\mathrm{e}^{-0.1t}. \quad (12)$$

2.2.2. Luminescent labels

If the reporter of a specific biological process is the catalyst of a luminescence reaction, the assay can be optimized in such a way that the rate-limiting factor becomes the catalyst concentration (Kricka, 1988). In such an assay, any

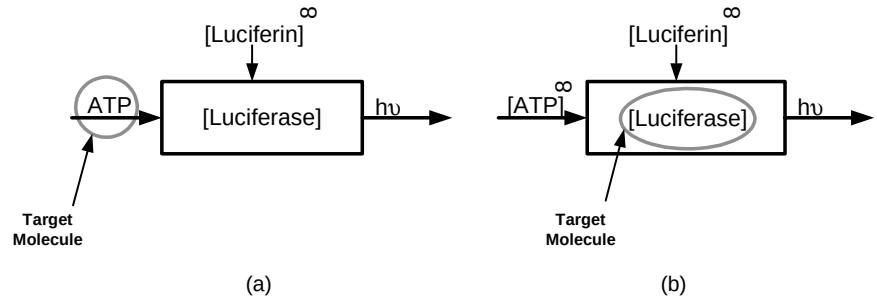

Fig. 3. Block diagram of (a) ATP detection assay and (b) luciferase detection system. The (∞) symbol indicates excess concentration.

change in target concentration changes the catalyst concentration, therefore altering the photon flux intensity as shown in Fig. 3b. The light intensity in the case where luciferase is the label of the target becomes

$$I(t) \approx 5.3 \times 10^{22} V[E_0]. \quad (13)$$

2.2.3. Pyrosequencing

Pyrosequencing is a DNA sequencing method based on the detection of released inorganic pyrophosphate during DNA synthesis. Using a linked enzymatic reaction, visible light (at 562 nm) proportional to the number of incorporated nucleotides is generated (Brovko et al., 1994; Ronaghi et al., 1996; Ronaghi, 2001). The enzymatic cascade begins with a DNA polymerization reaction in which inorganic pyrophosphate (PPi) is released as a result of nucleotide incorporation by polymerase. The released PPi is subsequently converted to ATP by ATP–sulfurylase. The synthesized ATP provides the energy for luciferase to generate photons. Unincorporated deoxy-nucleotides and ATP are degraded by the enzyme apyrase to chemically reset the enzymatic system after the incorporation test. The enzymatic reactions in this method are given by

$$(\mathrm{DNA})_n + \mathrm{dNTP} \xrightarrow{\text{Polymerase}} (\mathrm{DNA})_{n+1} + \mathrm{PPi} \quad (14)$$

$$\mathrm{PPi} + \mathrm{APS} \overset{\text{ATP–Sulfurylase}}{\leftrightarrow} \mathrm{ATP} + \mathrm{SO_4}^{-2} \quad (15)$$

$$\mathrm{ATP} + \text{luciferin} + \mathrm{O_2} \xrightarrow{\text{luciferase}} \mathrm{AMP} + \text{oxyluciferin} + \mathrm{CO_2} + \mathrm{PPi} + h\nu \quad (16)$$

$$\mathrm{dNTP} \xrightarrow{\text{Apyrase}} \mathrm{dNMP} + 2\mathrm{Pi}, \quad (17)$$

where APS is adenosine phosphosulfate, AMP, adenosine monophosphate, dNTP, deoxynucleotide triphosphate, and Pi, phosphate. As shown in Fig. 4 this enzymatic system regulates the light generation by recycling PPi, but the degrading enzyme, apyrase, breaks all nucleotide and ATP molecules in time, thus decreasing the light intensity. If we assume that PPi regulation has a unity gain positive feedback, and the turnover rate of apyrase is k_a, then the light generated by single incorporation from this bioluminometric assay is

$$I(t) = (\alpha VA) k_t [\mathrm{DNA}] \mathrm{e}^{-k_a t}. \quad (18)$$

For most practical applications, $k_a \approx 0.05\,\mathrm{s}^{-1}$ and $k_t \approx 1\,\mathrm{s}^{-1}$, and thus the light intensity becomes

$$I(t) = 5.3 \times 10^{23} V[\mathrm{DNA}] \mathrm{e}^{-0.05t}. \quad (19)$$

In (19) the negative effects of product inhibition are not included. While these unwanted pathways can potentially alter the kinetics of the reaction and the light intensity in general, one can still approximate light intensity in cases in which the sample concentration is low.

3. Detection system modeling

Having established a comprehensive model for the quantum efficiency of bioluminometric assays, we now discuss the detection portion of the system. Various detection systems have been developed for luminometry. By far the most sensitive detection devices are photomultiplier tubes (PMTs), which via a photocathode and a series of amplifying dynodes can generate up to one million electrons for every incident photon. These devices are very sensitive since their noise can be removed easily using a level-discriminator. However, they are costly and require high operating voltages (1000 VDC), precluding their use in a portable system. Furthermore, the overall photon detection efficiency of PMT-based systems is limited to 1–4% by the optics and the low quantum efficiency (10%) of PMTs. Finally, multiplexed imaging is not readily feasible using PMT's, as they are relatively large and thus unsuitable for dense arrays. It is this aspect of PMT's that has most limited their use and applicability (Van Dyke et al., 2002).

The most commonly used visible range imaging sensor architectures employ either charge-coupled device (CCD) or CMOS photosensor arrays. The major difference between the two is the specific readout mechanism used. CCDs employ a "bucket brigade" to serially shift out the photogenerated electrons accumulated at each photosite.

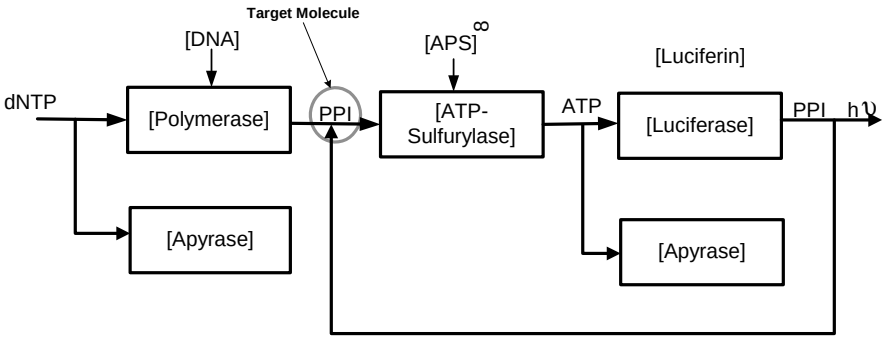

Fig. 4. Block diagram of pyrosequencing in which PPi released from DNA polymerization is measured. The (∞) symbol corresponds to excess concentration. Apyrase competes with polymerase and luciferase for dNTP and ATP consumption.

CCDs are fabricated in a nonstandard semiconductor process that is solely optimized for sensing and charge transfer (Holst, 1991). As a result, CCD image sensors achieve very high sensitivity, low noise, and low non-uniformity; hence they have earned a central place in the biological imaging arena. Although PMTs are more sensitive, unfortunately it has been our experience that ensuring the reliability of the chemistry itself places the true lower bound on detection requirements and thus CCDs do not have practical deficiencies in this respect. Since the thermal and shot noise generated from the photodiode junction cannot be differentiated from the photogenerated signal, cooling the device is the primary means of reducing such noise to negligible levels. Although liquid nitrogen is used in applications requiring extreme sensitivity (77 K), a lower cost and typically adequate solution involves incorporating a stack of Peltiers to cool the sensor down to as low as 200 K. This, however, requires the use of several high supply voltages resulting in high power consumption. Moreover, no other analog or digital circuits, such as for clock generation, timing, analog-to-digital (A/D) conversion, digital processing and storage, can be integrated with a CCD image sensor on a single chip resulting in multi-chip imaging system implementations with high power consumption, high cost, and large size.

CMOS, on the other hand, offers the benefits of CCDs with the possibilities of circumventing many of their drawbacks. For instance, CMOS offers complete customizability of the photodetection array to suit the requirements of the specific biological application. Hence the detection area of each photodiode can be optimally sized with respect to the assay volume and its light generation characteristics. Furthermore, this quality allows one to forego intermediary optics and to perform "contact" photonic detection of chemiluminescent assay signals, thereby drastically increasing photodetection efficiency to near *QE* limited percentages while eliminating expensive and bulky optics. This improvement alone can increase sensitivity of the system by an order of magnitude. Although others (Eggers et al., 1994; Lamture et al., 1994) performed such detection using a CCD-based sensor, it is the leveraged use of an integrated CMOS process that leads to considerable overall gains in system performance. More specifically, CMOS makes true low power operation possible, with the ability to integrate both the ADC and the DSP on chip enabling high quality detection combined with incomparable portability (El Gamal et al., 1999). Intelligent use of CMOS circuitry can be used to compensate for non-idealities engendered by the poorer quality (relative to CCDs) of added noise from the readout chain. Inclusion of transparent on-chip background subtraction and signal averaging circuitry are two examples that can help improve CMOS detection quality beyond that of CCD's. Background subtraction removes the deterministic thermally generated portion of the photodiode signal, leaving only its shot noise component that has a variance equal to the square root of its mean. Signal averaging lowers the independent noise components by $\sqrt{n}$, where n is the number of independent samples. Indeed, using CMOS as a biological platform has the potential of making "in the field" biological testing a reality.

A conceptual schematic of the proposed integrated system in which the chemistry is directly coupled to the CMOS-based detection chip is shown in Fig. 5a. A block diagram of the proposed detection chip is shown in Fig. 5b. It consists of a 2D array of pixels, each containing a photodetector and transistors for readout. The collected charge from each pixel is read out and converted in parallel to a digital format via an array of per-pixel analog-to-digital converters (ADCs). The system includes memory for on-chip storage of multiple frames. Moreover, a dedicated digital signal processor (DSP) is integrated on the chip to perform any needed computations, such as for background subtraction and read noise reduction. A detailed description of a prototype is provided in (Eltoukhy et al., 2004).

In Sections 3.1, 3.2 and 3.3 we describe the modeling and algorithms involved in the optics, image sensor and post-processing components of the detection chain.

3.1. Optics model

We first compare the optical efficiency of direct coupling to a conventional camera-based imaging system. Assuming

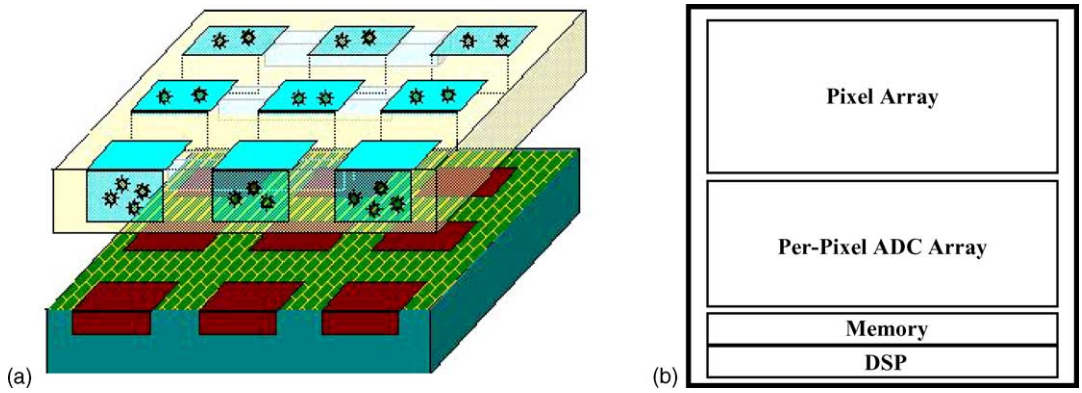

Fig. 5. (a) Conceptual schematic of the proposed integrated platform demonstrating the tight coupling between the sensor array and the biological assay reactions and (b) block diagram of the detection chip showing its main components.

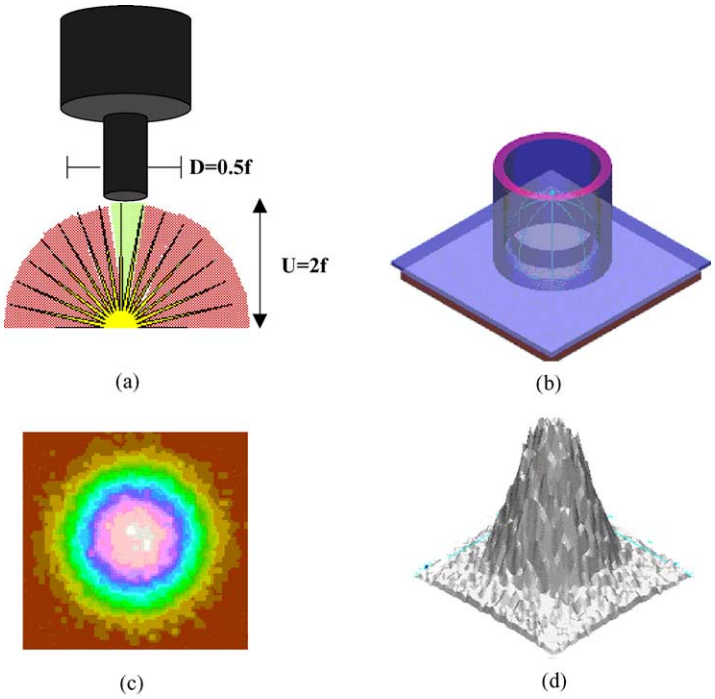

Fig. 6. (a) Model of light loss in camera-based system, (b) optical model of sensor-coupled assay, (c) simulated 2D sensor-plane intensity distribution, and (d) 3D sensor-plane intensity distribution.

that the object to be imaged is a point source located a distance U away from the lens (or the imaging surface in the case of direct coupling), the numerical aperture NA of the object side can be approximated using geometric optics by $\sin(\theta_{\max})$, where $\theta_{max} = tan^{-1}(D/2U)$ where D is the diameter of the lens aperture. Since optical efficiency (i.e. fraction of light collected by the lens) is proportional to $(NA)^2$, the efficiency of a camera-based system (see Fig. 6a) for typical parameter values of $D = 0.5\,f$ and $U = 2f$, where f, the focal length is a mere 1.6%. Optical efficiency can be greatly improved by directly coupling the chemistry to the detection chip surface as proposed in our integrated system. For example, taking $D = 100\,\mu m$ (photodetector size) and $U = 15\,\mu m$, the optical efficiency becomes 91%.

To accurately compute the optical efficiency for the direct coupling scenario, we use an optical simulator (LightTools^{TM}) and the specific luminescent assay and sensor parameters of the proposed setup to compute the point spread function, PSF (i.e. the function describing the distribution of light at the imaging plane due to a point source at the object plane). The PSF relates to the degree of blurring encountered in an optical system and can be used to calculate the resultant light intensity at the image plane due to the finite separation distance between the assay and the sensor. This is performed by convolving the derived PSF with the intensity distribution at the object plane to obtain the corresponding distribution at the imaging plane. Fig. 6b depicts a simplified model of the imaging setup and the simulated intensity distribution at the sensor plane is plotted in Figs. 6c and d.

3.2. Image sensor model

An image sensor comprises an array of pixels each having a photodetector and devices for readout. The sensor is typically operated in direct integration as illustrated in Fig. 7. Photons incident on the photodetector are converted into photocurrent. The photocurrent is directly integrated over the photodiode capacitance C_D into charge Q. The amount of charge that can be collected is limited by the well capacity Q_{max}. At the end of integration time T_{int}, the charge is read out as a voltage signal V_o, which is related to Q by the conversion gain g, i.e. $V_O = gQ$. Fig. 8 summarizes the overall image sensor model, including dark current, added shot and read noise, and the conversion gain.

The efficiency of converting incident photons to photocurrent $i_{ph}(t)$ is governed by the spectral response $\eta(\lambda)$ of the detector, where λ is the emission wavelength, and is given by

$$i_{ph}(t) = \eta(\lambda) I_{incident}(t). \tag{20}$$

Several sources contribute to noise during the collection of the photogenerated signal including dark current i_{dc} and photocurrent shot noise, reset noise, and readout noise. The total added average noise power can be expressed as

$$\sigma_n^2 = \tfrac{1}{q}(Q + Q_{dc}) + Q_{read}^2, \tag{21}$$

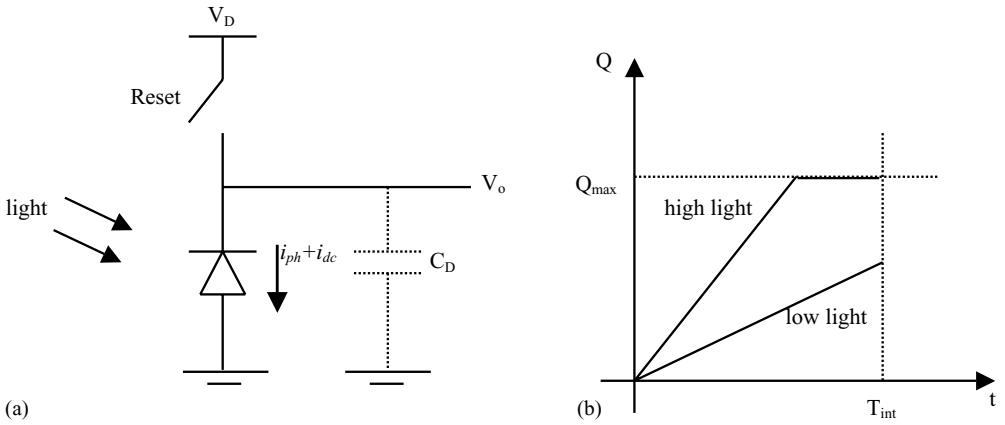

Fig. 7. (a) Simplified photodiode pixel model and (b) photocharge vs. time under different illumination conditions.

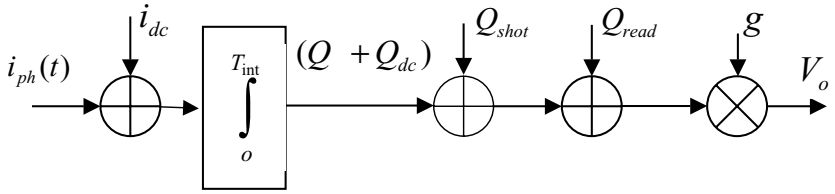

Fig. 8. Image sensor model, including added dark current, shot and read noises.

where the first term is the average power of the integrated shot noise of both the signal and the dark current, Q^2_{read} is the average read noise power, and $q = 1.602 \times 10^{-19}$ C. The signal-to-noise ratio, SNR, is defined as the ratio of the photogenerated signal power to the noise power and is given by

$$\text{SNR} = \frac{Q^2}{\sigma_n^2}. \tag{22}$$

3.3. Image post-processing

Once the image data is collected, post-processing algorithms can be applied to correct for non-idealities in both the optics and image sensor. For instance, the PSF can be used to correct for assay cross-talk using conventional equalization techniques, such as Weiner filtering. This enables higher throughput for the detection system, since tighter assay pitches can be tolerated. Fig. 9 shows an example of this filtering technique on an image with excessive cross-talk. Additionally, subtraction of both the chemical and detector backgrounds as well as digital accumulation incorporating the reaction kinetics can be performed to enhance SNR and, thus, detection reliability.

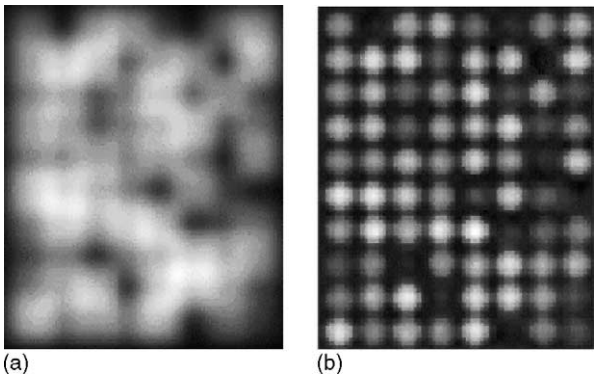

Fig. 9. Microarray image (a) before post-processing and (b) after applying cross-talk reduction algorithm.

4. Simulation and experimental results

By combining the models and algorithms discussed in the previous sections for the reaction kinetics, optical path, image sensor and post-processing, the minimum detectable analyte concentration can be estimated for a given set of detection system parameters. A block diagram of the luminescence detection system simulator that implements these models is shown in Fig. 10. The simulator, including the reaction kinetics and image sensor models, are coded in Matlab, while the optical efficiency and PSF for a given system geometry are calculated using LightTools™ and passed as arguments to the Matlab script.

To validate the above simulation model, we built an isolated imaging chamber for luminescence detection. The system employs an ultrasonic sprayer attached to a robotic

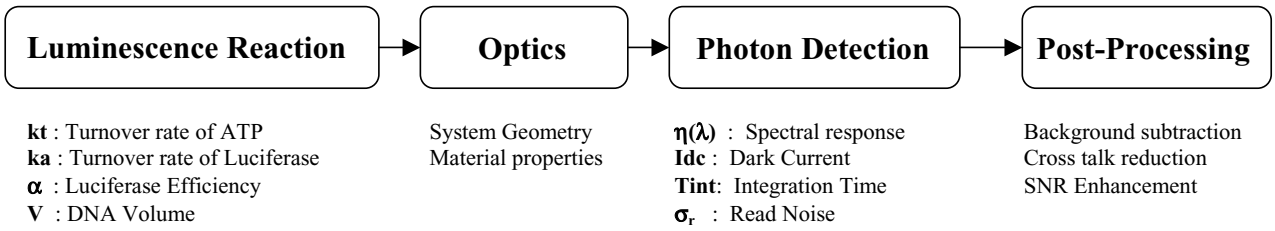

Fig. 10. Block diagram of luminescence detection system simulator.

arm for nucleotide and enzyme delivery to the target assays above the imaging apparatus as shown in Fig. 11. In order to simulate the types of conditions that would be encountered in an integrated CMOS detection system, a scientific-grade CCD (Hamamatsu HC230) is incorporated with the ultrasonic sprayer. The system allows direct placement of the assay slide onto the CCD. The CCD output is connected to a dedicated PC for simultaneously controlling the robotic arm of the sprayer, capturing images, and processing the assay data to achieve accurate detection. We implemented a simple but efficient algorithm for signal detection that can run in parallel with the data acquisition software. The algorithm automatically performs background subtraction of noise and utilizes line binning to increase SNR. An eight-tap low pass filter is utilized to smooth the resultant signal and remove any high frequency noise components. Also integrated with the script is an equalization routine for reduction of cross-talk using the modeled system PSF (see Fig. 12). This experimental setup allows for accurate measurement of the quantum efficiency of the reaction as well as of the optical and detection paths. The overall system dimensions are 50 cm × 50 cm × 60 cm due to the presence of the robotic arm. In contrast, the envisioned CMOS system under development will measure 10 cm × 10 cm × 2 cm.

We have used the experimental system to measure the light intensity produced during the incorporation of a single base in a Pyrosequencing reaction. Using 100 fmol of DNA per well, which is 10-fold lower than the amount currently used in commercial Pyrosequencing systems, we measured a peak signal-to-noise ratio of 750. We have also used the collected experimental data to fine-tune the parameters of the chemical kinetics, optics, and detector models. This "tuning" involved incorporating the specific association and disassociation rate constants, optical path loss, sensor noise characteristics, and overall system delay resulting from the finite mixing time of the sprayer. Fig. 13 compares the simulated and experimental results during incorporation of one nucleotide in a Pyrosequencing reaction using 100 fmol of DNA. As is readily seen, the simulation results are fairly well corroborated by the experimental data. Furthermore, using typical CMOS process parameter values at room temperature, our model predicts that 0.5 photon/s/μm^2 in conjunction with $T_{int} = 10$ s and 100 μm × 100 μm diode sizes would be needed to achieve a signal-to-noise ratio of 10. This implies that an integrated CMOS-based luminescence detection system would be capable of performing pyrosequencing with as little as 1 fmol of DNA, an amount three orders of magnitude lower than current commercial machines.

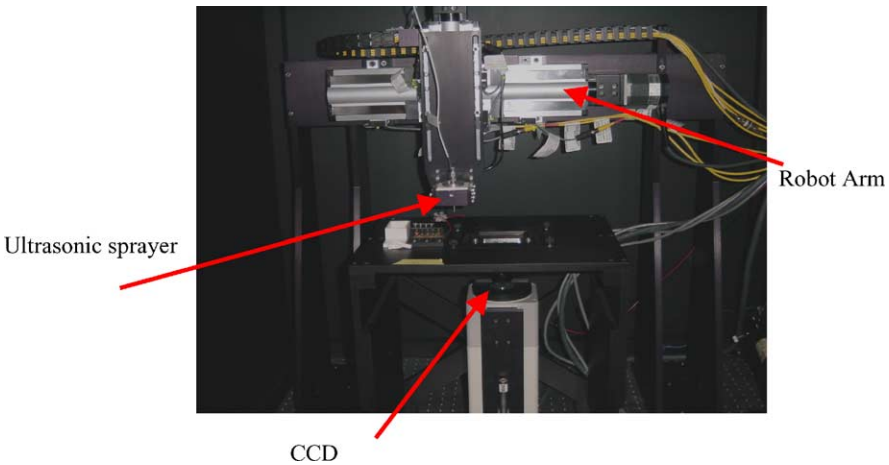

Fig. 11. Image of the prototype system including a robot-arm, an ultrasonic sprayer and a cooled CCD sensor.

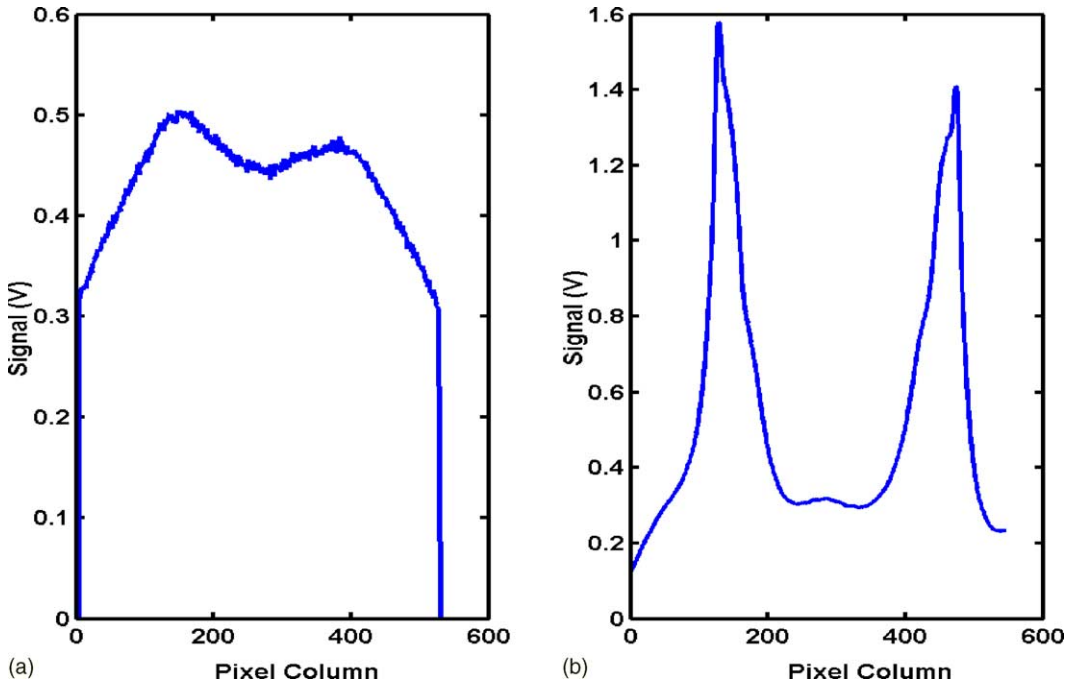

Fig. 12. (a) Plot of measured output signal voltage from each column of the CCD array for two adjacent 0.1 pmol wells and (b) same output after applying signal processing algorithms to reduce the effect of the system PSF.

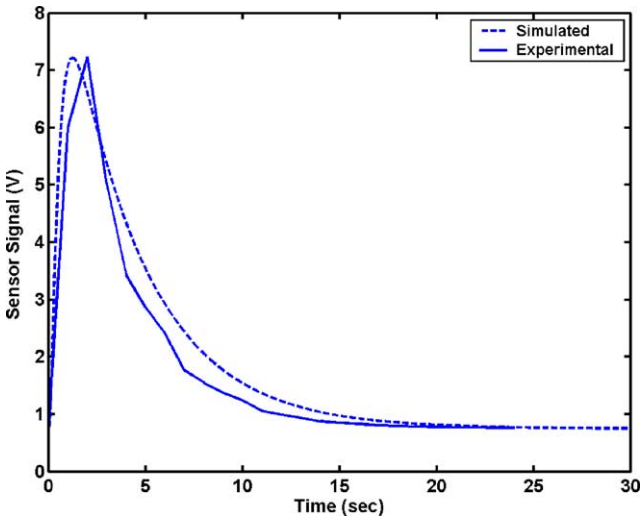

Fig. 13. Experimental data vs. combined chemistry and sensor simulation of detected signal vs. time of nucleotide incorporation in a Pyrosequencing reaction.

5. Conclusion

We described a simulation model for CCD and CMOS-based luminescence detection platforms. The model quantifies the photon flux generated by luminescence probes using ATP-based and luciferase label-based assay kinetics. The photon flux coupled with the system geometry is then used to calculate the incident photon flux on the imaging plane. Subsequently, the output image is computed using a detailed image sensor model. We constructed a prototype system to experimentally verify the developed models. Using this experimental setup we are able to obtain accurate measurements of the quantum efficiency, temporal kinetics and spatial distribution of the reaction, which are used to calculate the optimal assay sizes and throughput limits for the CMOS-based system.

Acknowledgements

The authors wish to thank Dr. M. Ronaghi, Dr. P. Griffin, Prof. R. Davis, A. Agah, A. Ercan, and S. Kavusi for their valuable insight and helpful discussions. We acknowledge the support of the Stanford Genome Technology Center in conducting most of the experimental work.

References

Brovko, L., Gandel'man, O., Polenova, T., Ugarova, N., 1994. Kinetics of bioluminescence in the firefly luciferin–luciferase System. Biochemistry 59, 195–201.

De Mello, A.J., 1996. Surface Analytical Technique for Probing Biomaterial Processes. CRC Press, Boca Raton/New York.

El Gamal, A., Yang, D., Fowler, B., 1999. Pixel-level processing—why, what and how. Proceedings of the SPIE 5650, pp. 2–13.

Eltoukhy, H., Salama, K., El Gamal, A., Ronaghi, M., Davis, R.W., 2004. A 0.18 μm CMOS 10^{-16} lux bioluminescence detection SoC. IEEE ISSCC Digest of Technical Papers 47.

Eggers, M., Hogan, M., Reich, R., Lamture, J., Ehrlich, D., Hollis, M., Kosicki, B., Powdrill, T., Beattie, K., Smith, S., Varma, R., Gangad-

haran, R., Mallik, A., Burke, B., Wallace, D., 1994. A microchip for quantitative detection of molecules utilizing luminescent and radioisotope reporter groups. Biotechniques 17 (3), 516–525.

Haugland, R.P., 1998. Handbook of Fluorescent Probes and Research Chemicals, Molecular Probes. Eugene, OR.

Holst, G., 1991. CCD Arrays, Cameras, and Displays, 2nd edition, SPIE Press.

Koster, H., Van Den Boom, D., Braun, A., Jacob, A., Jurinke, C., Little, D.P., Tang, K., 1997. DNA analysis by mass spectrometry: applications in DNA sequencing and DNA diagnostics. Nucleosides Nucleotides 16, 563–571.

Kricka, L.J., 1988. Clinical and biological applications of luciferases and luciferins. Anal. Biochem. 175, 14–22.

Kunz, R.E., 1997. Miniature integrated optical modules for chemical and biochemical sensing. Sens. Actuators B 38, 13–28.

Lamture, J.B., Beattie, K.L., Burke, B.E., Eggers, M.D., Ehrlich, D.J., Fowler, R., Hollis, M.A., Kosicki, B.B., Reich, R.K., Smith, S.R., 1994. Direct detection of nucleic acid hybridization on the surface of a charge coupled device. Nucl. Acids Res. 22 (11), 2121–2125.

Ronaghi, M., Karamohamed, S., Pettersson, B., Uhlen, M., Nyren, P., 1996. Real-time DNA sequencing using detection of pyrophosphate release. Anal. Biochem. 242, 84–89.

Ronaghi, M., 2001. Pyrosequencing sheds light on DNA sequencing. Genome Res. 11, 3–11.

Schena, M., Shalon, D., Davis, R.W., Brown, P.O., 1995. Quantitative monitoring of gene expression patterns with a cDNA microarray. Science 270, 467–470.

Tang, K., Fu, D., Kotter, S., Cotter, R.J., Cantor, C.R., Koster, H., 1995. Matrix-assisted laser desorption/ionization mass spectrometry of immobilized duplex DNA probes. Nucl. Acids Res. 23, 3126–3131.

Turner, G.K., 1985. Measurement of light from chemical or biochemical reactions. In: Van Dyke, N., Van Dyke, C., Woodfork, K., (Eds.), Bioluminescence and Chemiluminescence: Instruments and Applications, pp. 43–78.

Van Dyke, N., Van Dyke, C., Woodfork, K., (Eds.), 2002. Luminescence Biotechnology: Instruments and Applications. CRC Press, Boca Raton/New York.

Verpoorte, E., Manz, A., Ludi, H., Bruno, A.E., Maystre, F., Krattiger, B., Widmer, H.M., Van Der Schoot, B.H., De Rooij, N.F., 1992. A silicon flow cell for optical-detection in miniaturized total chemical-analysis systems. Sens. Actuators B 66 (6), 66–70.

Woolley, A.T., Lao, K., Glazer, A., Mathies, R.A., 1998. Capillary electrophoresis chips with integrated electrochemical detection. Anal. Chem. 70, 684–688.